

Distortion of the CMB spectrum by the first molecules of the Dark Ages

Yu. Kulinich and B. Novosyadlyj

Astronomical Observatory of Ivan Franko National University of Lviv, Kyryla i Methodia str., 8, Lviv, 79005, Ukraine
e-mail: yuriy.kulinich@lnu.edu.ua

April 1, 2025

ABSTRACT

Context. The formation of first stars and galaxies at the Cosmic Dawn had been preceded by the chain of primordial chemistry reactions during Dark Ages which generated first molecules, mostly H_2 , HD, and HeH^+ , so crucial for first stars to emerge. These molecules absorbed and scattered CMB quanta this way distorting CMB spectrum.

Aims. Estimate how much bound-bound transitions between the rovibrational levels of H_2 , HD, and HeH^+ molecules contribute to the distortion of CMB spectrum in the standard ΛCDM cosmology.

Methods. We describe the kinetics of the formation of the first molecules with system of 166 chemical reactions involving 20 reagents. The system of differential equations is solved to describe the processes of spontaneous and collisional transitions between rovibrational levels of H_2 , HD, and HeH^+ molecules. The populations of rovibrational levels and optical thickness of the gas in transition lines between these levels were used to estimate the differential brightness produced by the first molecules on the cosmic microwave background.

Results. It is shown that the signal from the first molecules in the standard ΛCDM cosmology takes the form of an absorption profile in the CMB spectrum and originates from the Dark Ages. The absorption profile of H_2 molecule: features multiple peaks; reaches maximum of $\sim 10^{-3}$ Jy/sr within the frequency range from ~ 50 GHz to ~ 120 GHz; and major contribution in absorption comes from redshifts $300 > z > 200$. The absorption profile of HD molecule: features double peaks; reaches maximum of $\sim 10^{-5}$ Jy/sr within the frequency range from ~ 40 GHz to ~ 70 GHz; and largest part of absorption comes from redshifts $300 > z > 30$. The absorption profile of HeH^+ ion-molecule: has no features and reaches maximum of $\sim 10^{-7}$ Jy/sr within the frequency range from ~ 200 GHz to ~ 800 GHz; and absorption comes mainly from redshifts range $100 > z > 4$.

Key words. CMB spectral distortions – primordial chemistry — Dark Ages

1. Introduction

Approximately 300,000 years (redshift $z \sim 1100$) after the Big Bang the plasma recombined and cosmic microwave background (CMB) photons had decoupled from baryonic matter, marking the beginning of the Dark Ages that lasted until the first stars and galaxies come to being at $z \sim 20 - 30$. During this time period, the Universe was filled with: CMB photons, dark matter (DM), dark energy (DE), and a weakly ionised gas, almost entirely made up of hydrogen ($\approx 92.4\%$ of total number density), helium-4 ($\approx 7.6\%$ (Aver et al. 2015)), along with trace amounts of deuterium ($\approx 2.45 \cdot 10^{-3}\%$ (Cooke et al. 2014)), as well as lithium-7 (as predicted by (Coc & Vangioni 2017) to amount to $\approx 5.61 \cdot 10^{-8}\%$ while observed (Sbordone et al. 2010) to be $\approx 1.58 \cdot 10^{-8}\%$). Also DM halos were formed from the initial over-density perturbations at the time, and primordial chemical reactions synthesized first molecules, with H_2 hydrogen molecules as most abundant (Latter & Black 1991; Lepp et al. 2002; Coppola et al. 2011; Longo et al. 2011), deuterium hydride molecules HD (Lepp et al. 2002; Glover & Abel 2008; Gay et al. 2011), helium hydride ion-molecule HeH^+ (Schleicher et al. 2008; Bovino et al. 2011b), and lithium hydride molecules LiH (Dalgarno et al. 1996; Stancil et al. 1996; Bougleux & Galli 1997; Schleicher et al. 2008; Stancil et al. 1996).

The estimation of fractions of the molecules is determined by the primordial chemistry model used, namely the set of chemi-

cal reactions and their rates as functions of gas, electron or radiation temperatures. The system of primordial chemistry equations can include as much as 300 reactions for about 30 reagents (Gay et al. 2011). However, besides the completeness of reaction set, the accuracy of molecular number predictions also depends on the accuracy of reactions' rates. Since any updates to the reaction chains and rates can affect the estimation of abundances, numerous attempts to trace chemical evolution during the Dark Ages have yielded quite different results, sometimes by orders of magnitude (Signore & Puy 2009; Bovino et al. 2009; Galli & Palla 1998; Galli & Palla 2002; Black 2006; Sethi et al. 2008; Puy & Signore 2007; Puy et al. 1993; Schleicher et al. 2008; Lepp et al. 2002; Lepp & Shull 1984). According to papers above, the absence of dust and heavy elements in the early Universe leads to extremely low molecular abundances. The fraction of molecules in the baryonic gas in relation to the cosmological background reaches $\sim 10^{-5} - 10^{-6}$ for hydrogen molecules, $\sim 10^{-9} - 10^{-10}$ for HD molecules, $\sim 10^{-11} - 10^{-14}$ for HeH^+ ion-molecules, and the fraction of LiH molecules reaches $\sim 10^{-20}$ at the end of the Dark Ages. In the Dark Matter halos chemical processes are expected to be more intense due to the denser and hotter environment. The number densities of H_2 and HD molecules at the moment of halo virialization are estimated as respectively $\sim 10^3$, it's ~ 400 times larger than that of uniformly expanding background, while the number density of HeH^+ ion molecules on the contrary appears to be of orders of magnitude

lower (Novosyadlyj et al. 2018, 2022). Despite quite low abundances of primordial molecules in early Universe they are a crucial ingredient for the formation of the first stars. Therefore, their detection will provide an important insight into the processes in early Universe that led to the emergence of the first stars, galaxies, and supermassive black holes.

Dark Ages are studied by detecting spectral distortions of the CMB caused by primordial chemistry and the 21 cm transition in neutral hydrogen. The idea that resonant scattering of CMB photons in the rovibrational lines of some primordial molecules of Dark Ages halos could lead to an observable signature in the CMB thermal spectrum was first proposed by Dubrovich (1977) in the late 1970s. Since then, a number of papers have analysed the possibility of detecting the resonant lines (e.g. Maoli et al. (1994, 1996); Basu (2007); Dubrovich et al. (2008)) and there have been three attempts to observe the effect, without success so far (Persson, C. M. et al. 2010; Gosachinskij et al. 2002; de Bernardis et al. 1993). Paper Schleicher et al. (2008) considers the distortion of CMB spectrum due to absorption, photoionization, and photo-dissociation processes during free-free and bound-free transitions involving atomic and molecular ions on the cosmological background of Dark Ages. There, most promising results were obtained for the negative hydrogen ion H^- and the HeH^+ ion-molecules. In this paper we have calculated the contribution to the distortion of the CMB spectrum by bound-bound transitions between rovibrational levels of the first molecules H_2 , HD, and HeH^+ . LiH molecules are not considered due to their low abundance.

2. Primordial chemistry

Primordial chemical reactions start at the epoch of recombination when neutral atoms emerged and continue in the post-recombination Universe due to the presence of residuals of free electrons and ions. The presence of such ingredients in almost neutral post-recombination gas triggers a chain of chemical reactions, thus leading to the synthesis of the first diatomic compounds, among which the most common are molecules H_2 and HD, as well as the helium hydride ion HeH^+ . They are expected to have played a crucial role in forming the first stars by allowing protostellar gas clouds to cool and collapse. However, as mentioned above the primordial gas was chemically depleted from atoms in various ionized and excited states. In our calculations, we took into account twenty most common reactants, namely photons of cosmic relic radiation (γ), e^- , H, H^+ , H^- , H_2 , H_2^+ , H_3^+ , He, He^+ , He^{++} , HeH^+ , D, D^- , D^+ , D_2 , D_2^+ , HD, HD^+ , and H_2D^+ . For these reagents, we consider 166 reactions listed in Table B.1 subdivided into three groups: reactions not involving He and D nuclei are labelled with the prefix “H_”, reactions involving He nuclei and not involving D nuclei are labelled with the prefix “He_”, reactions involving D nuclei are labelled with the prefix “D_”. The Table shows the rates of the reactions as a function of gas temperature, electron temperature, or radiation temperature. The description in the Table lists the publications where corresponding approximate expressions were obtained.

In the Table B.1 we present new approximate expressions for the reaction rates of H_2 and HeH^+ . The first one is calculated based on the cross-section from the online database¹. The second is our approximation to the combined data from Schauer et al. (1989) and Johnsen et al. (1980). Some reactions involving molecules are sensitive to their quantum state. For them, the Table B.1 contains reaction rates for two cases: $v = 0$ corresponds

to the case when the molecule is in the ground vibrational state, LTE corresponds to condition of local thermodynamic equilibrium for the population of rovibrational levels. Under conditions of early Universe the population of rotational and vibrational levels of molecules is mainly determined by the temperature of CMB radiation. At the same time, the frequency of collisions depends on the temperature of the gas. At redshifts $z > 200$, the gas and background radiation temperatures are equal, so it is correct to use LTE approximation. At lower redshifts, the gas temperature is slightly below the temperature of the background radiation, so the LTE approximation is less accurate though we continue to use it.

Since the density of the i -th reactant, n_i , changes not only due to chemical reactions but also due to the expansion of the Universe, it is convenient to represent the amount of the reactant in the form of a fraction, that is, relative to the total number of hydrogen nuclei as $x_i \equiv n_i/n_{\text{H}}$. The evolution of the fraction of the i -th reactant, x_i , is determined only by chemical reactions and is described by a kinetic equation that has the following general form (Puy et al. 1993; Galli & Palla 1998; Vonlanthen et al. 2009; Novosyadlyj et al. 2018):

$$\left(\frac{dx_i}{dt}\right)_{\text{chem}} = \sum_{mn} k_{mn}^{(i)} n_{\text{H}} x_m x_n + \sum_m k_{m\gamma}^{(i)} x_m - \sum_j k_{ij} n_{\text{H}} x_i x_j - k_{i\gamma} x_i, \quad (1)$$

where $k_{mn}^{(i)}$ is the reaction rate of reactants m and n with the formation of reactant i . The number of differential equations can be reduced by applying four equalities $1 = x_{\text{HI}} + x_{\text{HII}} + x_{\text{H}^-} + x_{\text{HD}} + x_{\text{HD}^+} + x_{\text{HeH}^+} + 2x_{\text{H}_2^+} + 2x_{\text{H}_2} + 2x_{\text{H}_2\text{D}^+} + 3x_{\text{H}_3^+}$, $x_{\text{D}} = x_{\text{DI}} + x_{\text{DII}} + x_{\text{HD}} + x_{\text{HD}^+} + x_{\text{H}_2\text{D}^+}$, $x_{\text{He}} = x_{\text{HeI}} + x_{\text{HeII}} + x_{\text{HeIII}} + x_{\text{HeH}^+}$, and $x_e = x_{\text{HII}} + x_{\text{DII}} + x_{\text{HeII}} + 2x_{\text{HeIII}} + x_{\text{H}_2^+} + x_{\text{D}_2^+} + x_{\text{HeH}^+} + x_{\text{H}_3^+} + x_{\text{HD}^+} + x_{\text{H}_2\text{D}^+} - x_{\text{H}^-}$.

In practice, we used the last equality to calculate the fraction of free electrons, while the others allowed us to control the accuracy of the integration of the differential equations. We did not calculate the change in the number of photons since, as noted above, the number of relic photons exceeds the number of photons arising from recombination by nine orders of magnitude. All calculations were performed for the period from the cosmological recombination up to hydrogen reionization at $z_{\text{rei}} \approx 6$ and for corresponding values of main parameters of the cosmological model as determined by final data release of the Planck Space Observatory (Planck Collaboration et al. 2020), listed in the previous section.

Main results of our calculations are shown in Fig. 1, where the relative abundances of representative species involved in the formation of H_2 (top left panel), HD (top right), and HeH^+ (bottom left panel) are given in units of hydrogen nucleus number density, deuterium nucleus number density, and helium nucleus number density, respectively. The relative abundances of first molecules in units of hydrogen nucleus number density are presented in the bottom right panel. Our results qualitatively reproduce the results of other authors, since the core of the most important reactions is common.

We have analysed chemical reactions for their influence on the chemistry of the early Universe from the moment of recombination to the moment of reionization. In the Table B.1, we have highlighted in bold those reactions that, in the indicated redshift range, give a maximum contribution to the synthesis or destruction of any of the reactants of more than 0.1 percent. Such an analysis shows which of the reactions played a noticeable role in the early Universe (within the framework of the standard cosmological model). It is assumed that in halos and cosmological

¹ <https://home.strw.leidenuniv.nl/~ewine/photo/>

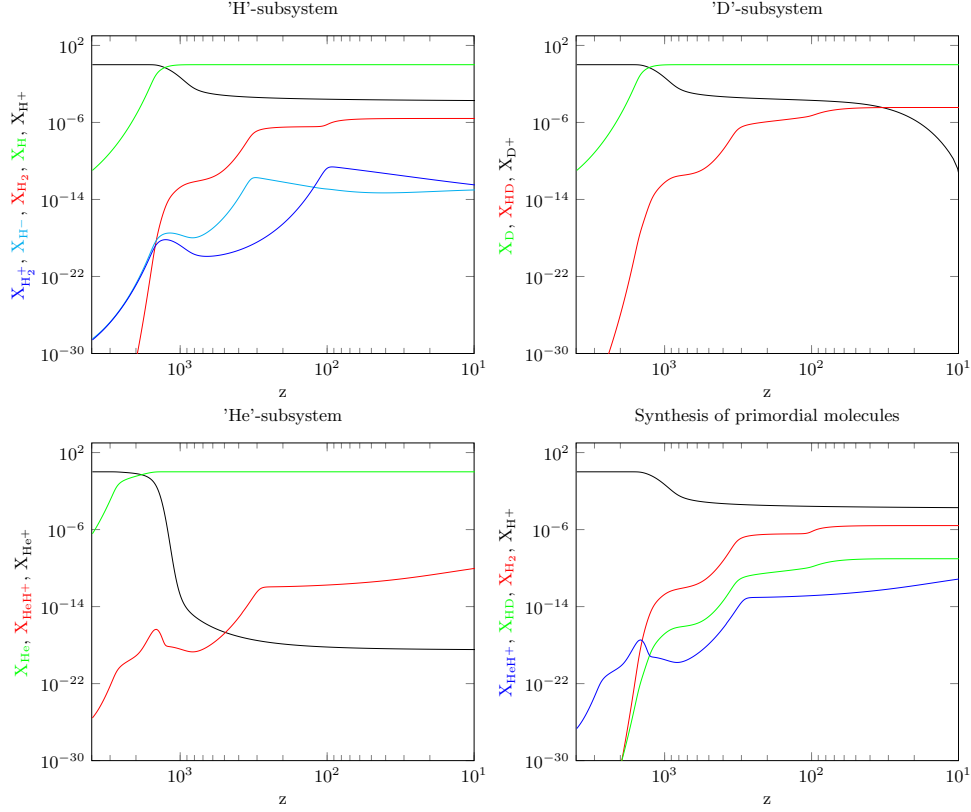


Fig. 1. Abundances of atoms, molecules, and ions across redshifts. Panels show relative abundances of key species for H_2 (top left), HD (top right), and HeH^+ (bottom left) in units of the density of hydrogen, deuterium, and helium nuclei, respectively. The bottom right panel displays the first molecules' abundances in hydrogen nucleus number density across redshifts.

models with additional sources of ionization and heating (primordial magnetic fields, decaying or annihilating dark matter particles, primordial black holes) this set will be somewhat different. The interactive chemical reaction map we propose (i.e. Table B.2) is a new way of visualizing a network of chemical reactions, allowing us to visually track which reactions are already included in the model of primordial chemistry, and which ones can or should still be included.

2.1. The Chemistry of H_2

Direct radiative association of two neutral hydrogen atoms in the ground states to form a hydrogen molecule is very unlikely (rate $\ll 10^{-25} \text{ cm}^3 \text{ s}^{-1}$ (Gould & Salpeter 1963)) since the emitted photon in this process must be a result of forbidden transition between the two Hitler-London states of the molecule. Direct radiative association of two neutral hydrogen atoms is possible if one of the two colliding atoms is in an excited state (say, in the $2p$ state), then the emission of photon will occur through an allowed transition between the two states of the molecule. However, the fraction of H atoms in the $2p$ and other excited states in the post-recombination Universe is so small that this process can be neglected. Therefore, in the conditions of the early Universe, two indirect channels of formation of hydrogen molecules dominate – one through the mediation of ion H^- :



and other through the mediation of ion-molecule H_2^+ :

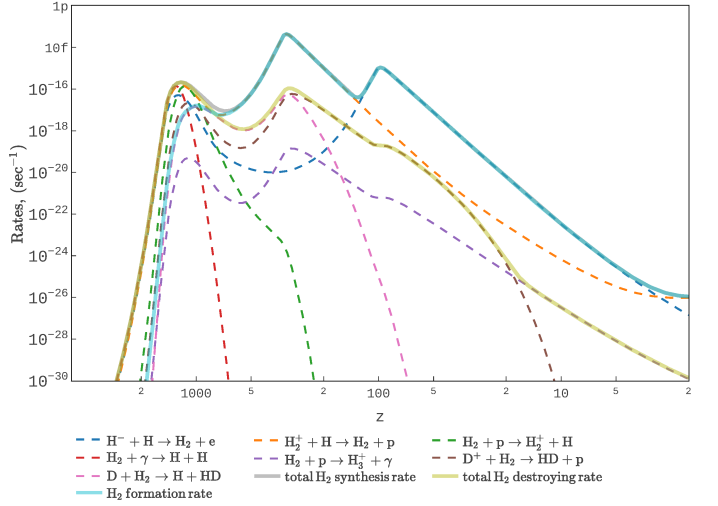


Fig. 2. Kinetics of formation and destruction of H_2 molecules. The dependencies of the rates of the main reactions involved in the formation and destruction of H_2 molecules are provided.

As shown in Fig.2, the former process dominates at $z \leq 127$ and reaches the maximum rates at the two peaks located at $z \approx 1270$ and $z \approx 98$. The second process dominates at $129 \leq z \leq 1400$, reaching peak efficiency at $z \approx 1220$ and $z \approx 320$. The gray and yellow lines in Fig.2 show the overall rates of synthesis and destruction of H_2 molecules, respectively, which takes into account all the involved reactions listed in Table B.1. The total formation rate is the difference between the

synthesis and destruction rates as shown in Fig. 2 by the solid cyan line. As can be seen from the figure, the formation of H_2 molecules at $z \geq 1050$ is an equilibrium process, while at lower redshifts, the rate of synthesis of H_2 molecules begins to prevail over their destruction.

The main channel for creating H^- ions is the process



The main channel for destruction H^- ions at $z \geq 100$ is process



while at $z \leq 100$, H^- ions are mainly spent on the formation of the H_2 molecule during the process (2). Since the formation of H^- ions is an equilibrium process in the early Universe, their number density can be easily estimated by the equality $k_{(4)}n_H n_{e^-} = n_{H^-}(k_{(5)} + k_{(2)}n_H)$, where $k_{(4)}$, $k_{(2)}$, and $k_{(3)}$ mark rates of processes (4), (2), and (5), respectively.

There are two main processes for formation of H_2^+ , the first of which



dominates at $z \leq 140$, while the second



dominates at $z \geq 140$. There are also two main processes for destruction of H_2^+ , the first of which



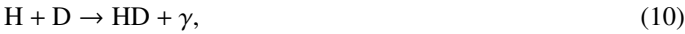
dominates at $z \leq 325$, while the second



dominates at $z \geq 325$. The formation of H_2^+ is an equilibrium process in the early Universe, and their number density can be easily estimated by the equality $k_{(6)}n_H n_{H^+} + k_{(7)}n_{HeH^+} n_H = n_{H_2^+}(k_{(8)} + k_{(9)}n_H)$, where $k_{(6)}$, $k_{(7)}$, $k_{(8)}$, and $k_{(9)}$ mark rates of processes (6), (7), (8), and (9), respectively.

2.2. The Chemistry of HD

Unlike H_2 , molecule of HD can be formed by direct radiative association of two neutral atoms in the process



which reaches its maximum efficiency in the epoch of recombination ($z \approx 1100$). However, two processes of formation of HD molecules from H_2 molecules are more effective in the conditions of the early Universe, namely charge transfer



and deuteron exchange



These processes have two peaks in efficiency at $z \approx 1180$ and $z \approx 307$ and dominate at $z \geq 20$. At a later time, as well as in the recombination epoch, processes involving H^- and D^- ions should also be considered, namely



and

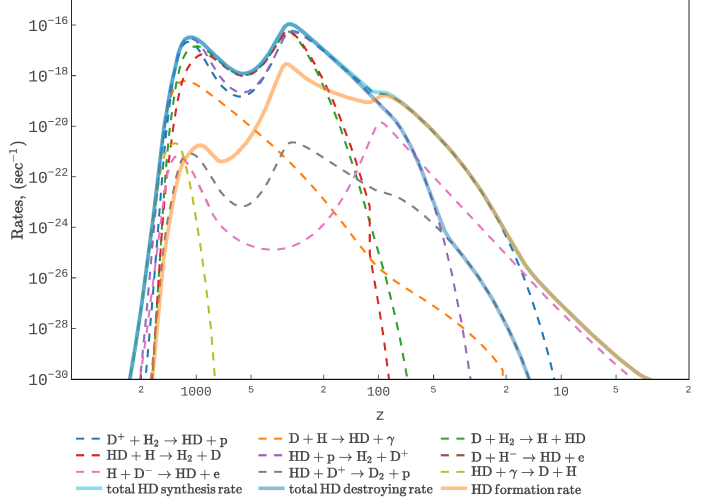


Fig. 3. Kinetics of formation and destruction of HD molecules. The dependencies of the rates of the main reactions involved in the formation and destruction of HD molecules are given.

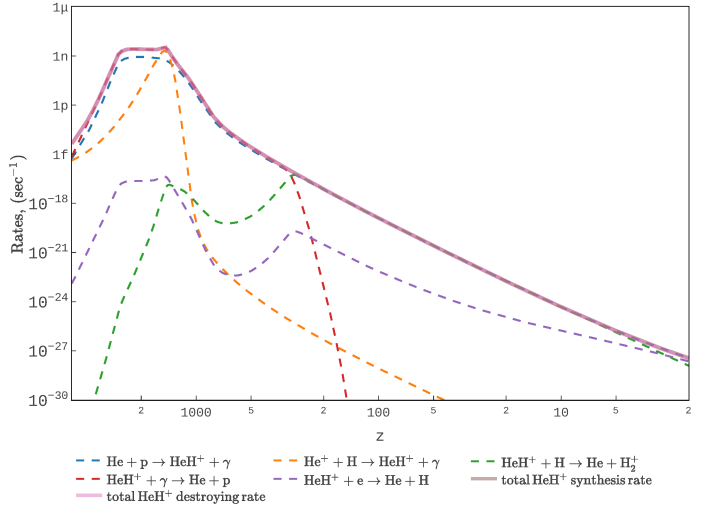


Fig. 4. Kinetics of formation and destruction of HeH^+ ion-molecules. The dependencies of the rates of the main reactions involved in the formation and destruction of HeH^+ ion-molecules are given.

The cyan and blue lines in Fig. 3 show the overall rates of synthesis and destruction of HD molecules when all reactions from Table B.1 are involved. The total formation rate is the difference between the synthesis and destruction rates and is shown in Fig. 3 by the solid orange line. As it follows from Fig. 3, the formation of HD molecule is an equilibrium process in early Universe at $z \geq 120$. At later stages of evolution ($z \leq 120$), the synthesis of HD molecules dominates over their destruction.

2.3. The Chemistry of HeH^+

As can be seen from Fig. 1 (see lower right panel), the helium hydride ion (HeH^+) was the first molecular ion that began to form in the early Universe during the recombination of He nuclei during the recombination epoch due to three processes



and



and



The main channel for destruction HeH^+ ion-molecules at $z \geq 300$ is process



while at $z \leq 300$, HeH^+ molecular ions were destroyed in collisions with neutral atoms of hydrogen due to process



The brown and pink lines in Fig. 4 show the overall rates of synthesis and destruction of HeH^+ molecules, taking into account all reactions listed in Table B.1. The fact that these lines merge in Fig. 4 means that the formation of HeH^+ molecules is an equilibrium process at all redshifts, and their number density can be estimated by the equality $k_{(15)}n_{\text{He}}n_{\text{H}^+} + (k_{(16)} + k_{(17)})n_{\text{He}^+}n_{\text{H}} = n_{\text{HeH}^+}(k_{(18)} + k_{(19)}n_{\text{H}})$, where $k_{(15)}$, $k_{(16)}$, $k_{(17)}$, $k_{(18)}$, and $k_{(19)}$ mark rates of processes (15), (16), (17), (18), and (19), respectively.

3. Rovibrational levels occupation

The kinetic equations for the population of rotational and vibrational levels are as follows

$$\begin{aligned} \frac{dX_{v,j}^m}{dt} = & \sum_s n_s \sum_{v',j'} \left[k_{v',j' \rightarrow v,j}^s X_{v',j'}^m - X_{v,j}^m k_{v,j \rightarrow v',j'}^s \right] \\ & + \left[\alpha_{v,j}^m \frac{d_+}{dt} - X_{v,j}^m \frac{d_-}{dt} \right] \ln(n_m a^3), \end{aligned} \quad (20)$$

where $X_{v,j}^m = n_{m,\{v,j\}} / \sum_{v',j'} n_{m,\{v',j'\}}$ is the fraction of molecules $m \in \{\text{H}_2, \text{HD}, \text{HeH}^+\}$ that is in the quantum state $\{v, j\}$, and the index $s \in \{\gamma, \text{H}, \text{p}, \text{e}\}$ indicates the collision partner of molecule m that caused the transitions. Here, we assume that the transitions between the rovibrational levels of Dark Age and Cosmic Down molecules are mainly due to the emission/absorption of photons, collisions with neutral hydrogen atoms, protons (responsible for ortho \leftrightarrow para transitions in H_2) and electrons (considered only for HeH^+). The last term of Eq. 20 describes the trend that population of rovibrational levels of newly synthesized molecules, $\alpha_{v,j}^m$, differs from the population of levels of molecules that have already been exposed to the environment, $X_{v,j}^m$. The former is obviously determined by the gas temperature,

$$\alpha_{v,j}^m \approx g_j \exp\{-E_{v,j}/k_B T\} / \sum_{v',j'} g_{j'} \exp\{-E_{v',j'}/k_B T\},$$

while the other is preferably determined by the CMB temperature. The derivative $d_+ \ln(n_m a^3)/dt$ specifies the rate of molecule synthesis, while derivative $d_- \ln(n_m a^3)/dt$ determines the rate of their destruction.

The main process to define the population of the rovibrational levels of the first molecules in the early Universe was collisions with quanta of cosmic microwave background radiation.

² The complete differential $d = d_+ - d_-$, where d_+ indicates an increase in the number of molecules due to their synthesis, and d_- means the destruction of molecules due to their destruction.

Table 1. Values of spontaneous rovibrational transitions allowed by quantum selection rules, along with frequencies and energy for the lowest rovibrational energy levels of para- and ortho-hydrogen molecules H_2 , hydrogen deuteride molecules HD, and helium hydride ion HeH^+ .

Species	Transitions ³ (v_u, j_u) - (v_l, j_l)	A_{ul} [s ⁻¹]	Frequency ν_{ul} [GHz]	E_u [K]
ortho-H ₂	1-0	-	-	170
	3-1	4.76×10 ⁻¹⁰	17 594	1 015
	5-3	9.83×10 ⁻⁹	31 011	2 503
	7-5	5.88×10 ⁻⁸	43 388	4 586
para-H ₂	2-0	2.94×10 ⁻¹¹	10 621	510
	4-2	2.75×10 ⁻⁹	24 410	1 681
	6-4	2.64×10 ⁻⁸	37 357	3 475
	8-6	1.14×10 ⁻⁷	49 077	5 830
HD	(0,1)-(0,0)	5.41×10 ⁻⁸	2 675	128
	(0,2)-(0,1)	5.13×10 ⁻⁷	5 332	384
	(0,3)-(0,2)	1.80×10 ⁻⁶	7 952	766
	(0,4)-(0,3)	4.31×10 ⁻⁶	10 518	1 271
	(0,5)-(0,4)	8.35×10 ⁻⁶	13 015	1 895
	(0,6)-(0,5)	1.40×10 ⁻⁵	15 429	2 636
	(0,7)-(0,6)	2.14×10 ⁻⁵	17 746	3 487
	(0,8)-(0,7)	3.03×10 ⁻⁵	19 955	4 445
	(1,0)-(0,1)	3.09×10 ⁻⁵	106 213	5 226
	(1,1)-(0,2)	1.55×10 ⁻⁵	103 441	5 349
	(1,1)-(0,0)	1.67×10 ⁻⁵	111 447	5 349
	(0,9)-(0,8)	4.07×10 ⁻⁵	22 055	5 503
	(1,2)-(0,1)	2.46×10 ⁻⁵	113 874	5 594
	(1,2)-(0,3)	1.01×10 ⁻⁵	100 590	5 594
(1,3)-(0,2)	3.16×10 ⁻⁵	116 150	5 959	
(1,3)-(0,4)	6.73×10 ⁻⁶	97 679	5 959	
(1,4)-(0,3)	3.86×10 ⁻⁵	118 259	6 442	
(1,4)-(0,5)	4.34×10 ⁻⁶	94 724	6 442	
(0,10)-(0,9)	5.23×10 ⁻⁵	24 038	6 657	
HeH ⁺	1-0	0.109	2 010	96
	2-1	1.04	4 009	289
	3-2	3.75	5 984	576
	4-3	9.14	7 925	956
	5-4	18.1	9 821	1 428

Since this radiation is a blackbody, the population of rovibrational levels can be considered to be in equilibrium with great accuracy, i.e., described by a Boltzmann distribution with temperature T_R . The contributions of spontaneous and radiative rovibrational transitions to the right-hand side of the equation (20) have the following form

$$n_\gamma \cdot k_{ul}^\gamma = A_{ul} + B_{ul} \cdot U(\nu_{ul}), \quad n_\gamma \cdot k_{lu}^\gamma = B_{lu} \cdot U(\nu_{ul}),$$

where index 'ul' means up to low levels transition whereas index 'lu' means low to up levels transition, A_{ul} is the rate of spontaneous emission, $B_{ul} = (c^3/4h\nu_{ul}^3)A_{ul}$ is the rate of radiative emission, $B_{lu} = B_{ul}$ is the rate of radiative absorption, and

$$U(\nu) = \frac{4h\nu^3}{c^3} \frac{1}{\exp(h\nu/kT_R) - 1}$$

is the blackbody energy density. The values of transition frequencies and energies for allowed spontaneous rovibrational transitions are listed in Table 1, for low rovibrational energy levels. Data for para- and ortho- hydrogen molecules H_2 are taken from Roueff et al. (2019), data for hydrogen deuteride molecules HD and helium hydride ion HeH^+ are taken from Amaral et al. (2019).

Spontaneous emission and radiative rovibrational transitions for diatomic molecules with non-zero electric dipole moments

(case for HD and HeH⁺) obey quantum selection rules $\Delta j = \pm 1$ and $\Delta v = \pm 1$. Hydrogen molecules are homonuclear diatomic molecules with a zero electric dipole moment. For this reason, it is two types of them depending on the relative orientation of the nuclear spins: ortho- and para-. Ortho-hydrogen molecules are those in which the spins of both nuclei (protons) point in the same direction, so their total spin is $I_n + I_n = 1$, where $I_n = 1/2$ is the spin of one nucleus (proton). Molecules of hydrogen in which spins of both nuclei are directing in opposite directions are called para-hydrogen, and their total spin is $I_n + I_n = 0$. Spontaneous emission and radiative rovibrational transitions do not lead to the mixing of these spin isomers of hydrogen molecules because they obey the quantum selection rules $\Delta j = \pm 2$ and $\Delta v = \pm 1$. Spin isomers of homonuclear diatomic molecules have distinct sequences of statistical weights of rotational levels, $g_j = g_n(2j + 1)$, which differ in nuclear statistical weights – $g_n = I_n(2I_n + 1)$ or $g_n = (I_n + 1)(2I_n + 1)$ depending on the parity of j and symmetries of the binding wave functions. Ortho-hydrogen corresponds to odd values of j , and its nuclear statistical weight is $g_n = 3$, while for para-hydrogen, with even values of j , nuclear statistical weight is $g_n = 1$. The statistical weight of any vibrational level v of a diatomic harmonic oscillator is $g_v = 1$.

The next factor affecting the population of the rovibrational levels of molecules is their collisions with the components of the baryon gas. As seen from Fig. 1, neutral hydrogen atoms used to be most abundant. In this paper, we used the collisional de-excitation rates, k_{ul} , of rovibrational levels of H₂ molecules by H given in Lique (2015), where u and l mean upper and lower rovibrational energy levels. The reverse transition rate (excitation) coefficients can be obtained as follows

$$k_{lu}(T) = \frac{g_u}{g_l} \exp\left\{-\frac{E_u - E_l}{k_B T}\right\} k_{ul}(T), \quad (21)$$

where E_u and E_l are the energies of the levels, g_u and g_l are statistical weights of the levels, and T is the baryon gas temperature. We used the rates from Desrousseaux et al. (2022) for collisional de-excitation of HD molecules by H. For collisional de-excitation of HeH⁺ molecules by H we used rates from Kulinich et al. (2020), which are somewhat higher than those obtained in Desrousseaux & Lique (2020). Although collisions of molecules H₂ with protons in the early Universe are much rarer, they nevertheless make a significant contribution to ortho-para transitions: $p + \text{H}_2(j) \leftrightarrow p + \text{H}_2(j')$, where $\Delta j = j' - j = \pm 1, \pm 2, \pm 3, \dots$. For collisional de-excitation of H₂ molecules by p , we used the rates from paper Gerlich (1990). Free electrons are faster than free protons, so their impact on the excitation and deactivation of the rotational levels of ion molecules HeH⁺ is more significant. To describe the rotational transitions in the helium hydride ion, HeH⁺, caused by collisions with free electrons, we used the transition rates from Khamesian et al. (2018), which unfortunately are only given for $j \leq 5$.

4. Global signals of the first molecules

During the Dark Ages, the temperature of baryonic matter is mainly determined by the competition between adiabatic cooling and heating due to the Compton scattering of CMBRs on free electrons. Other factors affecting the energy balance of the gas are collisional activations and de-activations of molecular rovibrational levels and primordial chemistry. However, as it shown in Puy et al. (1993); Novosyadlyj et al. (2023), these processes make a small contribution to the total energy balance of the gas in the cosmological background. Thus, energy balance for the

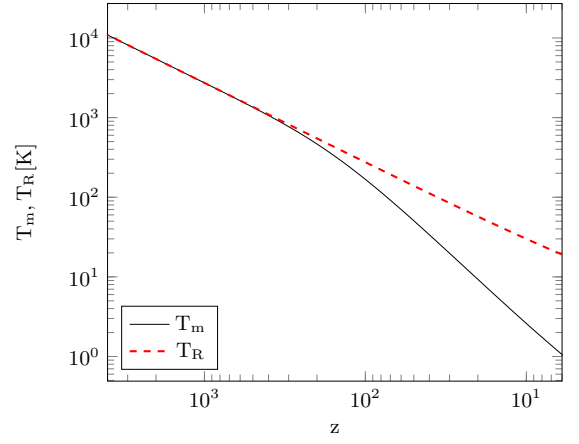


Fig. 5. Thermal history of the early Universe.

baryonic component on the cosmic background can be expressed by the equation of the evolution of its temperature with time

$$\frac{dT_m}{dt} = -2HT_m + \frac{8\sigma_T a T_R^4 (T_R - T_m) x_e}{3m_e c}, \quad (22)$$

where σ_T is the Thomson cross-section, a is the radiation constant, m_e is the electron mass, and x_e is the ionization fraction, n_b – is baryonic gas number density. Energy exchange between free electrons and the radiation field played a leading role in the early Universe, causing the equalization of baryon gas and radiation temperatures at redshifts $z > 300$ (see Fig. 5). At lower redshifts, the transfer of energy from radiation to the baryonic gas slows down significantly due to the reduced frequency of collisions between electrons and quanta of CMB radiation in the expanding Universe. From this moment on, adiabatic cooling begins to dominate, therefore baryon gas cooled faster than radiation.

Population of the rovibrational levels starts to deviate from the equilibrium at redshifts $z < 300$ due to collisions between molecules and other components of the baryon gas, where the temperature of the baryon gas is slightly lower than the temperature of the CMB radiation. These deviations can be represented as a deviation of the excitation temperature,

$$T_{ex}^{ul} \equiv \frac{E_u - E_l}{k_B} \ln^{-1} \left(\frac{g_u n_l}{g_l n_u} \right), \quad (23)$$

from the radiation temperature T_R . The differential brightness of the first molecules on the background of CMB can be expressed as

$$\delta I_{ul} = \frac{2h\nu_{ul}^3}{c^2} \left[\frac{1}{e^{\frac{h\nu_{ul}}{k_B T_{ex}} - 1}} - \frac{1}{e^{\frac{h\nu_{ul}}{k_B T_R} - 1}} \right] \tau_{ul},$$

where the optical depth in the transition lines $u \rightarrow l$ in the approximation of narrow line looks as follows

$$\tau_{ul} = \frac{1}{8\pi} \frac{\lambda_{ul}^3 A_{ul}}{H(z)} n_{\text{mol}} \left(X_l \frac{g_u}{g_l} - X_u \right),$$

where $\lambda_{ul} = c/\nu_{ul}$ is wavelength, $H(z)$ is expansion rate that depend on redshift, n_{mol} is number density of molecules. Note, we can not observe individual lines but their superposition

$$\delta I_{\text{tot}} = \sum_{\text{transitions}} \delta I_{ul}.$$

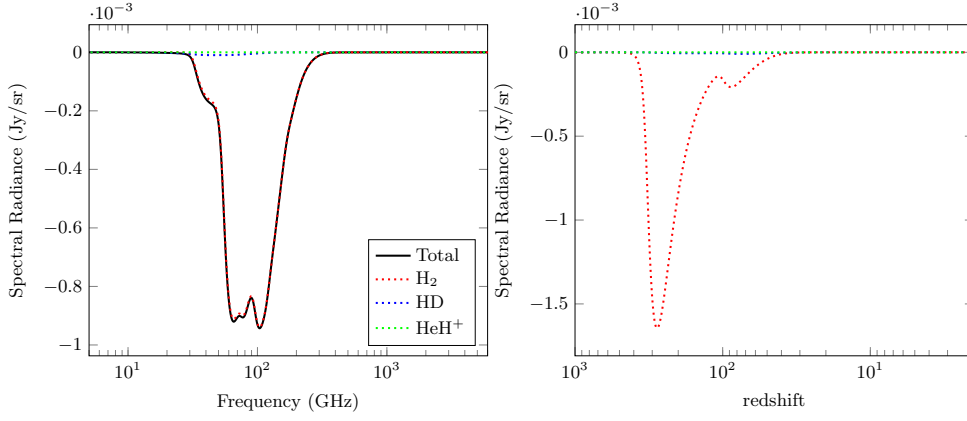


Fig. 6. Left panel: superposition of absorption profiles of the first molecules H_2 and HD, and ion-molecule HeH^+ . Right panel: redshifts at which absorption occurred.

Differential brightness of the molecules in the rovibrational lines, as well as their superposition, are shown in Fig. A.1, where the left panels show absorption profiles in the rotational lines of molecules H_2 (upper panel) and HD (middle panel), and ion-molecule HeH^+ (bottom panel). The dotted coloured lines show contributions from separate transitions, whereas the black line shows their superposition. The right panels on Fig. A.1 show the redshifts at which absorption occurred for corresponding transitions for H_2 (upper panel) and HD (middle panel) molecules and for ion-molecule HeH^+ (bottom panel). As you can see, absorption begins at $z \simeq 300$ when the gas temperature T starts to deviate from the CMB temperature T_R . The absorption profile of H_2 molecule has a multi-peak feature and reaches a maximum amplitude of $\sim 10^{-3}$ Jy/sr within the frequency range from about 50 GHz to about 120 GHz. The maximum absorption in rovibrational lines of H_2 molecules comes from redshifts $300 > z > 200$. The absorption profile of the HD molecule has a double peak feature and reaches a maximum amplitude of $\sim 10^{-5}$ Jy/sr within the frequency range of 40 GHz to 70 GHz. Maximal absorption in rovibrational lines of HD molecules comes from redshifts $300 > z > 30$. The absorption profile of HeH^+ ion-molecule has no features and reaches a maximum amplitude of $\sim 10^{-7}$ Jy/sr within the frequency range of 200 GHz to 800 GHz. The maximal contribution to absorption in rovibrational lines of HeH^+ ion-molecule comes from redshifts $100 > z > 4$.

The superposition of absorption profiles of the first molecules H_2 and HD, and ion-molecule HeH^+ is shown on the left panel of Fig. 6. As you can see, despite zero electric dipole moments of molecules H_2 , their absorption signal dominates over the HD absorption signal by two orders of magnitude and dominates over the HeH^+ absorption signal by four orders of magnitude. This happens due to a larger population of hydrogen molecules among all other compounds in the early post-recombination Universe (see Fig. 1). From the right panel of Fig. 6, one can see that molecular absorption occurs in the Dark Ages of the Universe (lie in the redshift range $1000 > z > 30$).

5. Discussion and conclusions

The global signal from first molecules is a useful source of information from yet undiscovered parts of the visible Universe. It can provide information about the thermal and ionization history of baryonic matter as well as the kinetics of primordial chemistry in the epoch of the Dark Ages. In standard cosmology, this signal takes a form of an absorption profile on the CMB spectrum.

Our estimates of the expected signal from H_2 and HD molecules are of two orders of magnitude lower for the H_2 case and three orders of magnitude lower for the HD case compared to the results of Puy et al. (1993). This discrepancy can be explained by the difference in cosmological models. In the model we used, the baryon abundance is only $\Omega_b = 0.0493$ in contrast to $\Omega_b = 1$ in Puy et al. (1993). The difference in results was also influenced by the difference in the models of primordial chemistry used. What is similar to our results is the position of the H_2 and HD signals in the CMB spectrum.

The effects of primordial chemistry on the CMB spectrum was previously studied also in Schleicher et al. (2008) where free-free and bound-free absorption and emission processes were considered for ions H^- and He^- as well as for ion-molecules HD^+ and HeH^+ . There, most promising results were obtained for the negative hydrogen ion H^- for which the relative change in the CMB temperature lies in the range $10^{-15} \lesssim \delta T_R/T_R \lesssim 10^{-6}$ for the frequency range of $10 \text{ GHz} < \nu < 2000 \text{ GHz}$ (see Fig. 10 in Schleicher et al. (2008)). The authors did not take into account absorption by H_2 and HD molecules, considering it to be relatively small.

To compare molecular absorption obtained here with the ionic absorption from Schleicher et al. (2008), we use the formula that relates small-amplitude intensity fluctuations to small-amplitude temperature fluctuations:

$$\frac{\delta I}{I} \approx f(x) \frac{\delta T_R}{T_R},$$

where $f(x) = x \cdot \exp(x)/(\exp(x) - 1)$, and $x = h\nu/k_B T_R$. At the frequency $\nu \approx 10^2$ GHz, where the absorption amplitude of first molecules is at maximum $\delta I \approx 0.9 \cdot 10^{-3}$ Jy/sr (see Fig. 6), the CMB specific intensity is equal to $I \approx 3 \cdot 10^8$ Jy/sr. For $\nu = 10^2$ GHz and $T_R \approx 2.7$ K we obtain $x \approx 1.7$ and $f(x) \approx 2.0$. Therefore, relative fluctuations of the CMB specific intensity at frequency $\nu = 10^2$ GHz is estimated at the level of $\delta I/I \approx 3 \cdot 10^{-12}$ in correspondence to relative fluctuations of the CMB temperature at the level of $\delta T_R/T_R \approx 1.5 \cdot 10^{-12}$. So the maximum of first molecules signal is located in the minimum of the signal from negative hydrogen ion (see Fig. 10 in Schleicher et al. (2008)), exceeding it by several orders of magnitude. This means that molecular absorption cannot be neglected in comparison to ionic absorption.

To assess the possibility of detecting a signal from the first molecules, other sources of the CMB spectrum distortion in the standard Λ CDM cosmology should be taken into account. These

are μ - and γ -distortions, a temperature shift due to a relative error of the measured CMB temperature $|\Delta T_R/T_R| \lesssim 5 \times 10^{-4}$, and the cosmological recombination radiation (Desjacques et al. 2015). The frequency dependencies of the first three are monotonic and well-determined so that they can be removed from the overall signal. The latter depends on the details of the recombination of H and He at $z \sim 10^3$ and has a non-monotonic character with excess CMB emission at the frequency of $\sim 10^2$ GHz at the level of $\sim 10^{-1}$ Jy/sr. These are two orders of magnitude larger than the signal from the first molecules.

Therefore, we conclude that detecting the signal from the first molecules will require the accuracy of predicting the cosmological recombination radiation up to the third order of magnitude, as well as a radio telescope with a sensitivity of $\sim 10^{-4}$ Jy/sr with spectral resolution of several tens of GHz.

Acknowledgements. We thank an anonymous referee whose comments significantly improved this article. This work is done in the framework of the project "Tomography of the Dark Ages and Cosmic Dawn in the lines of hydrogen and the first molecules as a test of cosmological models" (state registration number 0124U004029) supported by National Research Found of Ukraine. The authors are grateful to Pavlo Kopach for technical assistance in the preparation of the paper.

References

- Adams, N. G. & Smith, D. 1985, *ApJ*, 294, L63
 Albertsson, T., Indriolo, N., Kreckel, H., et al. 2014, *ApJ*, 787, 44
 Amaral, P. H. R., Diniz, L. G., Jones, K. A., et al. 2019, *ApJ*, 878, 95
 Aver, E., Olive, K. A., & Skillman, E. D. 2015, *JCAP*, 2015, 011
 Basu, K. 2007, *New Astron. Rev.*, 51, 431, francesco Melchiorri: Scientist, Pioneer, Mentor
 Black, J. H. 1978, *ApJ*, 222, 125
 Black, J. H. 2006, *Faraday Disc.*, 133, 27
 Bougleux, E. & Galli, D. 1997, *MNRAS*, 288, 638
 Bovino, S., Tacconi, M., Gianturco, F. A., & Galli, D. 2011b, *A&A*, 529, A140
 Bovino, S., Wernli, M., & Gianturco, F. A. 2009, *ApJ*, 699, 383
 Coc, A. & Vangioni, E. 2017, *Int. J. Mod. Phys. E*, 26, 1741002
 Cooke, R. J., Pettini, M., Jorgenson, R. A., Murphy, M. T., & Steidel, C. C. 2014, *ApJ*, 781, 31
 Coppola, C. M., Diomede, P., Longo, S., & Capitelli, M. 2011, *ApJ*, 727, 37
 Coppola, C. M., Kazandjian, M. V., Galli, D., Heays, A. N., & van Dishoeck, E. F. 2017, *MNRAS*, 470, 4163
 Coppola, C. M., Longo, S., Capitelli, M., Palla, F., & Galli, D. 2011, *ApJS*, 193, 7
 Coppola, C. M., Longo, S., Capitelli, M., Palla, F., & Galli, D. 2011, *ApJS*, 193, 7
 Courtney, E. D. S., Forrey, R. C., McArdle, R. T., Stancil, P. C., & Babb, J. F. 2021, *ApJ*, 919, 70
 Croft, H., Dickinson, A. S., & Gadea, F. X. 1999, *MNRAS*, 304, 327
 Dalgarno, A., Kirby, K., & Stancil, P. C. 1996, *ApJ*, 458, 397
 Dalgarno, A. & Lepp, S. 1987, in *IAU Symposium*, Vol. 120, *Astrochem.*, ed. M. S. Vardya & S. P. Tarafdar, 109–118
 Dalgarno, A. & McDowell, M. R. C. 1956, *Proc. Phys. Soc. A*, 69, 615
 Datz, S., Larsson, M., Stromholm, C., et al. 1995, *Phys. Rev. A*, 52, 2901
 de Bernardis, P., Dubrovich, V., Encrenaz, P., et al. 1993, *A&A*, 269, 1
 De Fazio, D. 2014, *PCCP*, 16, 11662
 Desjacques, V., Chluba, J., Silk, J., de Bernardis, F., & Doré, O. 2015, *MNRAS*, 451, 4460
 Desrousseaux, B., Coppola, C. M., & Lique, F. 2022, *MNRAS*, 513, 900
 Desrousseaux, B. & Lique, F. 2020, *J. Chem. Phys.*, 152, 074303
 Dickinson, A. S. 2005, *J. Phys. B Atom. Mol. Phys.*, 38, 4329
 Dove, J. E., Rusk, A. C. M., Cribb, P. H., & Martin, P. G. 1987, *ApJ*, 318, 379
 Dubrovich, V., Bajkova, A., & Khaikin, V. 2008, *New Astron.*, 13, 28
 Dubrovich, V. K. 1977, *Sov. Astron. Lett.*, 3, 128
 Ferland, G. J., Peterson, B. M., Horne, K., Welsh, W. F., & Nahar, S. N. 1992, *ApJ*, 387, 95
 Galli, D. & Palla, F. 1998, *A&A*, 335, 403
 Galli, D. & Palla, F. 2002, *P&SS*, 50, 1197
 Gay, C. D., Stancil, P. C., Lepp, S., & Dalgarno, A. 2011, *ApJ*, 737, 44
 Gerlich, D. 1990, *J. Chem. Phys.*, 92, 2377
 Glover, S. C. O. & Abel, T. 2008, *MNRAS*, 388, 1627
 Gosachinskij, I. V., Dubrovich, V. K., Zhelenkov, S. R., Il'in, G. N., & Prozorov, V. A. 2002, *Astron. Rep.*, 46, 543
 Gould, R. J. & Salpeter, E. E. 1963, *ApJ*, 138, 393
 Huq, M. S., Doverspike, L. D., Champion, R. L., & Esaulov, V. A. 1982, *J. Phys. B Atom. Mol. Phys.*, 15, 951
 Janev, R. K., Langer, W. D., Post, Douglas E., J., & Evans, Kenneth, J., eds. 1987, *Elementary processes in hydrogen-helium plasmas: Cross sections and reaction rate coefficients*, Vol. 4
 Janev, R. K., Reiter, D., & Samm, U. 2003, *Collision Processes in Low-Temperature Hydrogen Plasmas*, Tech. Rep. Jül-4105, Forschungszentrum Jülich GmbH, Jülich, Germany
 Johnsen, R., Chen, A., & Biondi, M. A. 1980, *J. Chem. Phys.*, 72, 3085
 Karpas, Z., Anicich, V., & Huntress, W. T. 1979, *J. Chem. Phys.*, 70, 2877
 Khamesian, M., Ayouz, M., Singh, J., & Kokoouline, V. 2018, *Atoms*, 6, 49
 Kimura, M., Lane, N. F., Dalgarno, A., & Dixon, R. G. 1993, *ApJ*, 405, 801
 Kulinich, Y., Novosyadlyj, B., Shulga, V., & Han, W. 2020, *Phys. Rev. D*, 101, 083519
 Larsson, M., Lepp, S., Dalgarno, A., et al. 1996, *A&A*, 309, L1
 Latter, W. B. & Black, J. H. 1991, *ApJ*, 372, 161
 Lepp, S. & Shull, J. M. 1983, *ApJ*, 270, 578
 Lepp, S. & Shull, J. M. 1984, *ApJ*, 280, 465
 Lepp, S., Stancil, P. C., & Dalgarno, A. 2002, *J. Phys. B: Atom., Mol. Opt. Phys.*, 35, R57
 Linder, F., Janev, R. K., & Botero, J. 1995, in *Atomic and Molecular Processes in Fusion Edge Plasmas*, ed. R. K. Janev, 397
 Lindinger, W., Howorka, F., Maerk, T., & Egger, F. 1982, in *Symposium on Atomic and Surface Phys.*, 1982 Contrib.
 Lique, F. 2015, *MNRAS*, 453, 810
 Longo, S., Coppola, C. M., Galli, D., Palla, F., & Capitelli, M. 2011, *Rendiconti Lincei*, 22, 119
 Mac Low, M. M. & Shull, J. M. 1986, *ApJ*, 302, 585
 Maoli, R., Ferrucci, V., Melchiorri, F., Signore, M., & Tosti, D. 1996, *ApJ*, 457, 1
 Maoli, R., Melchiorri, F., & Tosti, D. 1994, *ApJ*, 425, 372
 Martin, P. G., Keogh, W. J., & Mandy, M. E. 1998, *ApJ*, 499, 793
 Méndez, I., Gordillo-Vázquez, F. J., Herrero, V. J., & Tanarro, I. 2006, *JPC A*, 110, 06060
 Mielke, S. L., Peterson, K. A., Schwenke, D. W., et al. 2003, *Phys. Rev. Lett.*, 91, 063201
 Novosyadlyj, B., Kulinich, Y., Melekh, B., & Shulga, V. 2022, *A&A*, 663, A120
 Novosyadlyj, B., Kulinich, Y., Milinevsky, G., & Shulga, V. 2023, *MNRAS*, 526, 2724
 Novosyadlyj, B., Shulga, V., Han, W., Kulinich, Y., & Tszih, M. 2018, *ApJ*, 865, 38
 Peart, B. & Hayton, D. A. 1994, *J. Phys. B Atom. Mol. Phys.*, 27, 2551
 Persson, C. M., Maoli, R., Encrenaz, P., et al. 2010, *A&A*, 515, A72
 Planck Collaboration, Aghanim, N., Akrami, Y., et al. 2020, *A&A*, 641, A6
 Poulaert, G., Brouillard, F., Claeys, W., McGowan, J. W., & Van Wassenhove, G. 1978, *J. Phys. B Atom. Mol. Phys.*, 11, L671
 Puy, D., Alecian, G., Le Bourlot, J., Leorat, J., & Pineau Des Forets, G. 1993, *A&A*, 267, 337
 Puy, D. & Signore, M. 2007, *New Astron. Rev.*, 51, 411
 Ramaker, D. E. & Peek, J. M. 1976, *Phys. Rev. A*, 13, 58
 Roueff, E., Abgrall, H., Czachorowski, P., et al. 2019, *A&A*, 630, A58
 Savin, D. W. 2002, *ApJ*, 566, 599
 Savin, D. W., Krstić, P. S., Haiman, Z., & Stancil, P. C. 2004, *ApJ*, 607, L147
 Sbordone, L., Bonifacio, P., Caffau, E., et al. 2010, *A&A*, 522, A26
 Schauer, M. M., Jefferts, S. R., Barlow, S. E., & Dunn, G. H. 1989, *J. Chem. Phys.*, 91, 4593
 Schleicher, D. R. G., Galli, D., Palla, F., et al. 2008, *A&A*, 490, 521
 Schulz, G. J. & Asundi, R. K. 1967, *Phys. Rev.*, 158, 25
 Seager, S., Sasselov, D. D., & Scott, D. 1999, *ApJ*, 523, L1
 Sethi, S. K., Nath, B. B., & Subramanian, K. 2008, *MNRAS*, 387, 1589
 Shapiro, P. R. & Kang, H. 1987, *ApJ*, 318, 32
 Shavitt, I. 1959, *J. Chem. Phys.*, 31, 1359
 Signore, M. & Puy, D. 2009, *EPJ C*, 59, 117
 Soon, W. H. 1992, *ApJ*, 394, 717
 Stancil, P. C., Lepp, S., & Dalgarno, A. 1996, *ApJ*, 458, 401
 Stancil, P. C., Lepp, S., & Dalgarno, A. 1998, *ApJ*, 509, 1
 Stromholm, C., Schneider, I. F., Sundström, G., et al. 1995, *Phys. Rev. A*, 52, R4320
 Theard, L. P. & Huntress, W. T. 1974, *J. Chem. Phys.*, 60, 2840
 Trevisan, C. S. & Tennyson, J. 2002a, *Plasma Phys. and Control. Fusion*, 44, 1263
 Trevisan, C. S. & Tennyson, J. 2002b, *Plasma Phys. and Control. Fusion*, 44, 2217
 Vonlanthen, P., Rauscher, T., Winteler, C., et al. 2009, *A&A*, 503, 47
 Walkauskas, L. & Kaufman, F. 1975, *Symposium (International) on Combustion*, 15, 691, fifteenth Symposium (International) on Combustion
 Walmsley, C. M., Flower, D. R., & Pineau des Forêts, G. 2004, *A&A*, 418, 1035
 Wang, J. G. & Stancil, P. C. 2002, *Phys. Scr.*, T96, 72
 Wishart, A. W. 1979, *MNRAS*, 187, 59P
 Xu, Y. & Fabrikant, I. I. 2001, *APL*, 78, 2598
 Zygelman, B., Dalgarno, A., Kimura, M., & Lane, N. F. 1989, *Phys. Rev. A*, 40, 2340

Appendix A: Absorption signals of H_2 , HD, and HeH^+

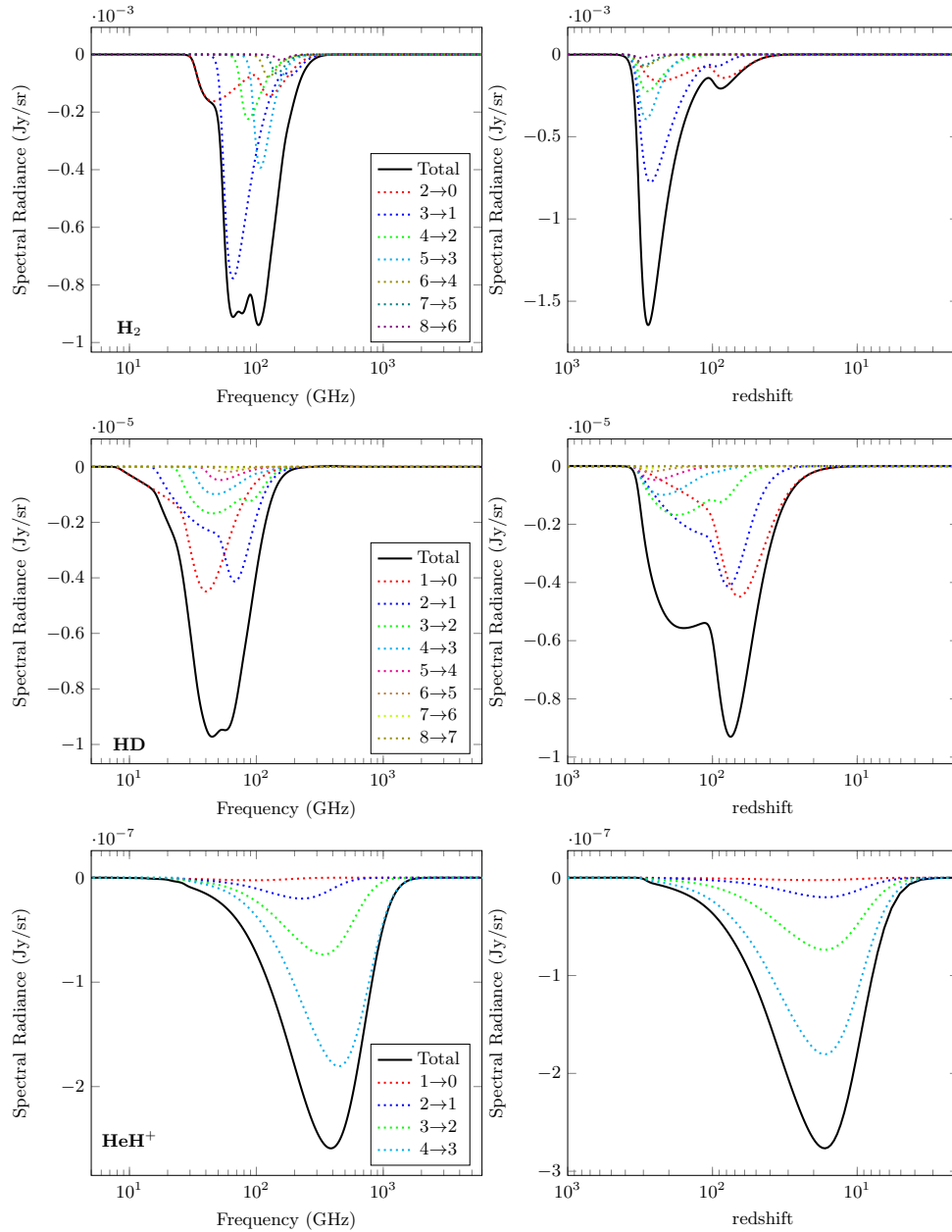


Fig. A.1. Left panels: absorption signal in the rotational lines of molecules H_2 (upper row), HD (middle row), and HeH^+ (bottom row) – dotted coloured lines show contributions from separate transitions, and the black line shows their superposition. Right panels: redshifts at which absorption occurred for corresponding transitions.

Table B.1 – continued from previous page

Tag	Reaction	Rate coefficient (cm ³ s ⁻¹ , cm ⁶ s ⁻¹ , s ⁻¹)		Ref.
H_26	H ₂ ⁺ + γ → 2H ⁺ + e ⁻	90.07 _R ^{1.48} exp(-335000.0/T _R)		3
H_27	H ₂ + e ⁻ → H ⁻ + H	2.7 × 10 ⁻⁸ T ^{-1.27} exp(- $\frac{43000}{T}$)		19
H_28	H ₂ + e ⁻ → H + H + e ⁻	4.49 × 10 ⁻⁹ T ^{0.11} exp(- $\frac{101858}{T}$)	v = 0	20
		1.91 × 10 ⁻⁹ T ^{0.136} exp(- $\frac{53407.1}{T}$)	LTE	20
H_29	H ₂ + H ₂ → H ₂ + H + H	$\frac{5.996 \times 10^{-30} T^{4.1881}}{(1.0 + 6.761 \times 10^{-6} T)^{5.6881}}$ exp(- $\frac{54657.4}{T}$)	v = 0	21
		1.3 × 10 ⁻⁹ exp(- $\frac{53300}{T}$)	LTE	22
H_30	H ₂ + He → H + H + He	dex[-27.029 + 3.801 log T - $\frac{29487}{T}$]	v = 0	23
		dex[-2.729 - 1.75 log T - $\frac{23474}{T}$]	LTE	23
H_31	H ⁻ + e ⁻ → H + e ⁻ + e ⁻	exp[-1.801849334 × 10 ¹ + 2.36085220 × 10 ⁰ ln T _{eV} - 2.82744300 × 10 ⁻¹ (ln T _{eV}) ² + 1.62331664 × 10 ⁻² (ln T _{eV}) ³ - 3.36501203 × 10 ⁻² (ln T _{eV}) ⁴ + 1.17832978 × 10 ⁻² (ln T _{eV}) ⁵ - 1.65619470 × 10 ⁻³ (ln T _{eV}) ⁶ + 1.06827520 × 10 ⁻⁴ (ln T _{eV}) ⁷ - 2.63128581 × 10 ⁻⁶ (ln T _{eV}) ⁸]		14
H_32	H ⁻ + H → H + H + e ⁻	2.5634 × 10 ⁻⁹ T _{eV} ^{1.78186} exp[-2.0372609 × 10 ¹ + 1.13944933 × 10 ⁰ ln T _{eV} - 1.4210135 × 10 ⁻¹ (ln T _{eV}) ² + 8.4644554 × 10 ⁻³ (ln T _{eV}) ³ - 1.4327641 × 10 ⁻³ (ln T _{eV}) ⁴ + 2.0122503 × 10 ⁻⁴ (ln T _{eV}) ⁵ + 8.6639632 × 10 ⁻⁵ (ln T _{eV}) ⁶ - 2.5850097 × 10 ⁻⁵ (ln T _{eV}) ⁷ + 2.4555012 × 10 ⁻⁶ (ln T _{eV}) ⁸ - 8.0683825 × 10 ⁻⁸ (ln T _{eV}) ⁹]	T _{eV} ≤ 0.1 eV T _{eV} > 0.1 eV	14
H_33	H ⁻ + H ₂ ⁺ → H ₂ + H	1.4 × 10 ⁻⁷ ($\frac{T}{300}$) ^{-0.5}		24
H_34	H ⁻ + H ₂ ⁺ → H + H + H	1.4 × 10 ⁻⁷ ($\frac{T}{300}$) ^{-0.5}		24
H_35	H + H + H ₂ → H ₂ + H ₂	0.143 × 10 ⁻³¹ T ^{-0.38}	T < 300 K	18
		0.486 × 10 ⁻³⁰ T ⁻¹	T ≥ 300 K	18
H_36	H + H + He → H ₂ + He	6.9 × 10 ⁻³² T ^{-0.4}		25
H_37	H ₂ ⁺ + H → 2H + H ⁺	exp(-32.912 + 6.9498 × 10 ⁻⁵ T - 3.3248 × 10 ⁴ /T - 4.08 × 10 ⁻⁹ T ²)		9
H_38	H ₂ + H ⁺ → 2H + H ⁺	exp(-33.404 + 2.0148 × 10 ⁻⁴ T - 5.2674 × 10 ⁴ /T - 1.0196 × 10 ⁻⁸ T ²)		9
H_39	H ₃ ⁺ + H ₂ → H ₃ ⁺ + 2H	0.3 × 10 ⁻¹⁰ ($\frac{T}{300}$) ^{0.5} exp(- $\frac{52000}{T}$)		26
H_40	H ₃ ⁺ + e ⁻ → H ₂ ⁺ + H + e ⁻	4.8462 × 10 ⁻⁷ T _{eV} ^{-0.04975} exp(- $\frac{19.165665}{T_{eV}}$)		16
H_41	H ₂ ⁺ + e ⁻ → H ⁺ + H + e ⁻	1.0702 × 10 ⁻⁷ T _{eV} ^{0.04876} exp(- $\frac{9.69028}{T_{eV}}$)		16
H_42	H + H → H + H ⁺ + e ⁻	1.45 × 10 ⁻¹⁵ T ^{0.5} (1.0 + $\frac{T}{26280}$) exp(- $\frac{78841}{T}$)		27
H_43	H ⁺ + H + H → H ₃ ⁺ + H	1.238 × 10 ⁻²⁹ T ^{-1.046}		17
H_44	H ₃ ⁺ + H ⁻ → H ₂ + H ₂	2.3 × 10 ⁻⁷ ($\frac{T}{300}$) ^{-0.5}		28
He_01	He ⁺ + e ⁻ → He + γ	k _{rec} = C _{HeI} · α _{HeI} ; α _{HeI} = q [√ $\frac{T_M}{T_2}$ (1 + √ $\frac{T_M}{T_2}$) ^{1-p} (1 + √ $\frac{T_M}{T_1}$) ^{1+p}] ⁻¹ m ³ s ⁻¹ , q = 10 ^{-16.744} , p = 0.711, T ₁ = 10 ^{5.114} K, T ₂ = 3 K. C _{HeI} = $\frac{(1 + K_{HeI} \Lambda_{He} n_{HeI} \exp(-E_{2p2s}/k_B T_M))}{(1 + K_{HeI} (\Lambda_{He} + \beta_{HeI}) n_{HeI} \exp(-E_{2p2s}/k_B T_M))}$, β _{HeI} = α _{HeI} · $\frac{1}{4} (2\pi m_e k_B T_M / h^2)^{3/2} \exp(-E_{2s}/k_B T_M)$ K _{HeI} ≡ λ _{Lyα} ³ / (8πH(z)), λ _{Lyα} = 58.4334 nm, Λ _{He} = 51.3 s ⁻¹ . E _{2p2s} = 9.64908313 × 10 ⁻²⁰ J, E _{2s} = 6.363254 × 10 ⁻¹⁹ J		1
He_02	He + γ → He ⁺ + e ⁻	k _{ion} = C _{HeI} · β _{HeI} exp(-E _{2s1s} /k _B T _M); E _{2s1s} = 3.30301387 × 10 ⁻¹⁸ J		1
He_03	He + H ⁺ → HeH ⁺ + γ	1.56 × 10 ⁻²⁰ ($\frac{T}{300}$) ^{-0.374} exp(- $\frac{T}{46000}$) + 11.8 × 10 ⁻²⁰ ($\frac{T}{300}$) ^{-0.244} exp(- $\frac{T}{2890}$)		29
He_04	HeH ⁺ + H → He + H ₂ ⁺	1.27228 × 10 ⁻⁹ (1.0 + 0.904409 $\frac{207.632}{8.314472T}$) ^{-1.0/0.904409}		30
He_05	HeH ⁺ + γ → He + H ⁺	2.03097 × 10 ⁸ T _R ^{-1.20281} exp(- $\frac{24732}{T_R}$)		31
He_06	He ⁺⁺ + e ⁻ → He ⁺ + γ	k _A = 2.538 × 10 ⁻¹³ ($\frac{1262456}{T}$) ^{1.503} × [1.0 + ($\frac{2418500}{T}$) ^{0.470}] ^{-1.923} k _B = 5.506 × 10 ⁻¹⁴ ($\frac{1262456}{T}$) ^{1.500} × [1.0 + ($\frac{460752}{T}$) ^{0.407}] ^{-2.242}	Case A	32
			Case B	32

Continued on next page

Table B.1 – continued from previous page

Tag	Reaction	Rate coefficient (cm ³ s ⁻¹ , cm ⁶ s ⁻¹ , s ⁻¹)		Ref.
He_07	$\text{He}^+ + \gamma \rightarrow \text{He}^{++} + \text{e}^-$	$50.07_R^{1.63} \exp\left(-\frac{590000.0}{T_R}\right)$		3
He_08	$\text{He} + \text{H}^+ \rightarrow \text{He}^+ + \text{H}$	$1.26 \times 10^{-9} T^{-0.75} \exp\left(-\frac{127500}{T}\right)$ $4.0 \times 10^{-37} T^{4.74}$	$T \leq 10000 \text{ K}$ $T > 10000 \text{ K}$	33
He_09	$\text{He}^+ + \text{H} \rightarrow \text{He} + \text{H}^+$	$1.2 \times 10^{-15} \left(\frac{T}{300}\right)^{0.25}$		34
He_10	$\text{He} + \text{H}_2^+ \rightarrow \text{HeH}^+ + \text{H}$	$3.0 \times 10^{-10} \exp\left(-\frac{6717.0}{T}\right)$		35
He_11	$\text{He}^+ + \text{H} \rightarrow \text{HeH}^+ + \gamma$	$4.16 \times 10^{-16} T^{-0.37} \exp\left(-\frac{T}{87600}\right)$		59
He_12	$\text{HeH}^+ + \text{e}^- \rightarrow \text{He} + \text{H}$	$3.0 \times 10^{-8} T^{-0.5}$		28
He_13	$\text{HeH}^+ + \text{H}_2 \rightarrow \text{H}_3^+ + \text{He}$	1.80×10^{-9}		28
He_14	$\text{HeH}^+ + \gamma \rightarrow \text{He}^+ + \text{H}$	$273518 T_R^{0.623525} \exp\left(-\frac{144044.0}{T_R}\right)$		31
He_15	$\text{He} + \text{e}^- \rightarrow \text{He}^+ + 2\text{e}^-$	$\exp[-4.409864886 \times 10^1$ $+ 2.391596563 \times 10^1 \ln T_{\text{eV}}$ $- 1.07532302 \times 10^1 (\ln T_{\text{eV}})^2$ $+ 3.05803875 \times 10^0 (\ln T_{\text{eV}})^3$ $- 5.68511890 \times 10^{-1} (\ln T_{\text{eV}})^4$ $+ 6.79539123 \times 10^{-2} (\ln T_{\text{eV}})^5$ $- 5.00905610 \times 10^{-3} (\ln T_{\text{eV}})^6$ $+ 2.06723616 \times 10^{-4} (\ln T_{\text{eV}})^7$ $- 3.64916141 \times 10^{-6} (\ln T_{\text{eV}})^8]$		14
He_16	$\text{He}^+ + \text{e}^- \rightarrow \text{He}^{++} + 2\text{e}^-$	$\exp[-6.87104099 \times 10^1$ $+ 4.393347633 \times 10^1 \ln T_{\text{eV}}$ $- 1.84806699 \times 10^1 (\ln T_{\text{eV}})^2$ $+ 4.70162649 \times 10^0 (\ln T_{\text{eV}})^3$ $- 7.6924663 \times 10^{-1} (\ln T_{\text{eV}})^4$ $+ 8.113042 \times 10^{-2} (\ln T_{\text{eV}})^5$ $- 5.32402063 \times 10^{-3} (\ln T_{\text{eV}})^6$ $+ 1.97570531 \times 10^{-4} (\ln T_{\text{eV}})^7$ $- 3.16558106 \times 10^{-6} (\ln T_{\text{eV}})^8]$		14
He_17	$\text{He}^+ + \text{H}^- \rightarrow \text{He} + \text{H}$	$2.32 \times 10^{-7} \left(\frac{T}{300}\right)^{-0.52} \exp\left(-\frac{T}{22400}\right)$		36
He_18	$\text{He} + \text{H}^+ + \gamma \rightarrow \text{HeH}^+ + 2\gamma$	$0.130 \times 10^{-20} \left(\frac{T}{300}\right)^{0.408} \exp\left(-\frac{T}{36400}\right)$ $+ 7.89 \times 10^{-20} \left(\frac{T}{300}\right)^{-0.399} \exp\left(-\frac{921}{T}\right)$		35
He_19	$\text{H}_2 + \text{He}^+ \rightarrow \text{He} + \text{H} + \text{H}^+$	$10^{-13} \cdot (-0.4732142857 + 0.0369047619 \cdot T$ $- 0.1488095 \cdot 10^{-3} \cdot T^2)$ $10^{-13} \cdot (1.623809524 - 0.1587301587 \cdot 10^{-2} \cdot T)$ $10^{-13} \cdot (0.111111524 + 0.1555555413 \cdot 10^{-2} \cdot T$ $+ 4.4444444 \cdot 10^{-6} \cdot T^2)$	$T < 78 \text{ K}$ $78 \text{ K} \leq T < 330 \text{ K}$ $T \geq 330 \text{ K}$	37
He_20	$\text{H}_2 + \text{He}^+ \rightarrow \text{H}_2^+ + \text{He}$	7.2×10^{-15}		38
He_21	$\text{He} + \text{H}^- \rightarrow \text{He} + \text{H} + \text{e}^-$	$4.1 \times 10^{-17} T^2 \exp\left(-\frac{19870}{T}\right)$		39
He_22	$\text{He}^+ + \text{H}_2 \rightarrow \text{He}^+ + 2\text{H}$	$0.3 \times 10^{-10} \left(\frac{T}{300}\right)^{0.5} \exp\left(-\frac{52000}{T}\right)$		26
D_01	$\text{D}^+ + \text{e}^- \rightarrow \text{D} + \gamma$	the same as for H_01		
D_02	$\text{D} + \gamma \rightarrow \text{D}^+ + \text{e}^-$	the same as for H_02		
D_03	$\text{D} + \text{H}^+ \rightarrow \text{H} + \text{D}^+$	$2.0 \times 10^{-10} T^{0.402} \exp\left(-\frac{37.1}{T}\right)$ $- 3.31 \times 10^{-17} T^{1.48}$ $3.44 \times 10^{-10} T^{0.35}$	$T \leq 2 \cdot 10^5 \text{ K}$ $T > 2 \cdot 10^5 \text{ K}$	40
D_04	$\text{H} + \text{D}^+ \rightarrow \text{D} + \text{H}^+$	$2.06 \times 10^{-10} T^{0.396} \exp\left(-\frac{33}{T}\right)$ $+ 2.03 \times 10^{-9} T^{-0.332}$		40
D_05	$\text{H}_2 + \text{D}^+ \rightarrow \text{HD} + \text{H}^+$	$[0.417 + 0.846 \log T - 0.137(\log T)^2] \times 10^{-9}$		41
D_06	$\text{HD} + \text{H}^+ \rightarrow \text{H}_2 + \text{D}^+$	$1.1 \times 10^{-9} \exp\left(-\frac{488}{T}\right)$		41
D_07	$\text{H} + \text{D} \rightarrow \text{HD} + \gamma$	$10^{-25} [2.80202 - 6.63697 \ln T$ $+ 4.75619(\ln T)^2 - 1.39325(\ln T)^3$ $+ 0.178259(\ln T)^4 - 0.00817097(\ln T)^5]$ $10^{-25} \exp[507.207 - 370.889 \ln T$ $+ 104.854(\ln T)^2 - 14.4192(\ln T)^3$ $+ 0.971469(\ln T)^4 - 0.0258076(\ln T)^5]$	$T \leq 200 \text{ K}$ $T > 200 \text{ K}$	42
D_08	$\text{H}_2 + \text{D} \rightarrow \text{HD} + \text{H}$	$\text{dex} [-56.4737 + 5.88886 \log T$ $+ 7.19692(\log T)^2$ $+ 2.25069(\log T)^3$ $- 2.16903(\log T)^4$ $+ 0.317887(\log T)^5]$	$T \leq 2000 \text{ K}$	43
D_09	$\text{HD}^+ + \text{H} \rightarrow \text{HD} + \text{H}^+$	$3.17 \times 10^{-10} \exp\left(-\frac{5207}{T}\right)$	$T > 2000 \text{ K}$	
D_10	$\text{HD} + \text{H} \rightarrow \text{H}_2 + \text{D}$	the same as for H_09 $5.25 \times 10^{-11} \exp\left(-\frac{4430}{T}\right)$ $5.25 \times 10^{-11} \exp\left(-\frac{4430}{T} + \frac{173900}{T^2}\right)$	$T \leq 200 \text{ K}$ $T > 200 \text{ K}$	44
D_11	$\text{D} + \text{H}^+ \rightarrow \text{HD}^+ + \gamma$	$3.9 \times 10^{-19} \left(\frac{T}{300}\right)^{1.8} \exp\left(\frac{20}{T}\right)$		45

Continued on next page

Table B.1 – continued from previous page

Tag	Reaction	Rate coefficient (cm ³ s ⁻¹ , cm ⁶ s ⁻¹ , s ⁻¹)		Ref.
D_12	$\text{H} + \text{D}^+ \rightarrow \text{HD}^+ + \gamma$	$3.9 \times 10^{-19} \left(\frac{T}{300}\right)^{1.8} \exp\left(\frac{20}{T}\right)$		45
D_13	$\text{HD}^+ + \gamma \rightarrow \text{H} + \text{D}^+$	the same as for H_08		
D_14	$\text{HD}^+ + \text{e}^- \rightarrow \text{H} + \text{D}$	$7.2 \times 10^{-8} T^{-0.5}$		46
D_15	$\text{HD}^+ + \text{H}_2 \rightarrow \text{H}_2\text{D}^+ + \text{H}$	the same as for H_13		
D_16	$\text{D} + \text{H}_3^+ \rightarrow \text{H}_2\text{D}^+ + \text{H}$	$4.55 \times 10^{-10} \left(\frac{T}{300}\right)^{-0.5} \exp\left(-\frac{900}{T}\right)$		28
D_17	$\text{H}_2\text{D}^+ + \text{e}^- \rightarrow 2\text{H} + \text{D}$	$0.73 \times 10^{-6} / \sqrt{T}$		47
D_18	$\text{H}_2\text{D}^+ + \text{e}^- \rightarrow \text{H}_2 + \text{D}$	$0.07 \times 10^{-6} / \sqrt{T}$		47
D_19	$\text{H}_2\text{D}^+ + \text{e}^- \rightarrow \text{HD} + \text{H}$	$0.20 \times 10^{-6} / \sqrt{T}$		47
D_20	$\text{H}_2\text{D}^+ + \text{H} \rightarrow \text{H}_3^+ + \text{D}$	$2.0 \times 10^{-8} T^{-1} \exp\left(-\frac{632}{T}\right)$		58
D_21	$\text{HD}^+ + \text{H} \rightarrow \text{H}_2^+ + \text{D}$	$1.0 \times 10^{-9} \exp\left(-\frac{154}{T}\right)$		48
D_22	$\text{D} + \text{H}^- \rightarrow \text{HD} + \text{e}^-$	7.5×10^{-10}	$T < 300$	49
		$2.0 \times 10^{-9} T^{-0.17}$	$T \geq 300$	49
D_23	$\text{H} + \text{D}^- \rightarrow \text{HD} + \text{e}^-$	7.5×10^{-10}	$T < 300$	49
		$2.0 \times 10^{-9} T^{-0.17}$	$T \geq 300$	49
D_24	$\text{HD} + \text{H}^+ \rightarrow \text{H}_2^+ + \text{D}$	$1.0 \times 10^{-9} \exp\left(-\frac{21600}{T}\right)$		50
D_25	$\text{HD}^+ + \text{H} \rightarrow \text{H}_2 + \text{D}^+$	1.0×10^{-9}		50
D_26	$\text{HD}^+ + \gamma \rightarrow \text{H}^+ + \text{D}$	the same as for H_08		
D_27	$\text{H}_2^+ + \text{D} \rightarrow \text{HD}^+ + \text{H}$	$1.07 \times 10^{-9} \left(\frac{T}{300}\right)^{0.062} \exp\left(-\frac{T}{41400}\right)$	$T \leq 6000 \text{ K}$	51
D_28	$\text{D} + \text{e}^- \rightarrow \text{D}^- + \gamma$	$\text{dex}[-17.845 + 0.762 \log T + 0.1523(\log T)^2 - 0.03274(\log T)^3]$ $\text{dex}[-16.4199 + 0.1998(\log T)^2 - 5.447 \times 10^{-3}(\log T)^4 + 4.0415 \times 10^{-5}(\log T)^6]$	$T > 6000 \text{ K}$	2
D_29	$\text{H} + \text{D}^- \rightarrow \text{D} + \text{H}^-$	$6.4 \times 10^{-9} \left(\frac{T}{300}\right)^{0.41}$		48
D_30	$\text{D} + \text{H}^- \rightarrow \text{H} + \text{D}^-$	$6.4 \times 10^{-9} \left(\frac{T}{300}\right)^{0.41}$		48
D_31	$\text{D} + \text{D}^- \rightarrow \text{D}_2 + \text{e}^-$	the same as for H_05		
D_32	$\text{H}^+ + \text{D}^- \rightarrow \text{HD}^+ + \text{e}^-$	$1.1 \times 10^{-9} \left(\frac{T}{300}\right)^{-0.4}$		45
D_33	$\text{D}^+ + \text{H}^- \rightarrow \text{HD}^+ + \text{e}^-$	$1.1 \times 10^{-9} \left(\frac{T}{300}\right)^{-0.4}$		45
D_34	$\text{D}^+ + \text{D}^- \rightarrow \text{D}_2^+ + \text{e}^-$	$1.3 \times 10^{-9} \left(\frac{T}{300}\right)^{-0.4}$		45
D_35	$\text{H}^+ + \text{D}^- \rightarrow \text{D} + \text{H}$	$2.4 \times 10^{-6} (1.0 + T/20000) / \sqrt{T}$		52
D_36	$\text{D} + \text{D}^+ \rightarrow \text{D}_2^+ + \gamma$	$1.9 \times 10^{-19} T_3^{1.8} \exp\left(\frac{20}{T}\right)$		45
D_37	$\text{D} + \text{H}_2^+ \rightarrow \text{H}_2 + \text{D}^+$	the same as for H_09		
D_38	$\text{H}_2^+ + \text{D} \rightarrow \text{HD} + \text{H}^+$	1.0×10^{-9}		50
D_39	$\text{HD}^+ + \text{D} \rightarrow \text{D}_2^+ + \text{H}$	1.0×10^{-9}		53
D_40	$\text{HD}^+ + \text{D} \rightarrow \text{D}_2 + \text{H}^+$	1.0×10^{-9}		50
D_41	$\text{H} + \text{D}_2^+ \rightarrow \text{D}_2 + \text{H}^+$	the same as for H_09		
D_42	$\text{D}_2^+ + \text{H} \rightarrow \text{HD}^+ + \text{D}$	$1.0 \times 10^{-9} \exp\left(-\frac{472}{T}\right)$		53
D_43	$\text{D}_2^+ + \text{H} \rightarrow \text{HD} + \text{D}^+$	1.0×10^{-9}		50
D_44	$\text{HD} + \text{D}^+ \rightarrow \text{D}_2 + \text{H}^+$	1.0×10^{-9}		53
D_45	$\text{D}_2 + \text{H}^+ \rightarrow \text{HD}^+ + \text{D}$	$\left[5.18 \times 10^{-11} + 3.05 \times 10^{-9} \left(\frac{T}{10000}\right) - 5.42 \times 10^{-10} \left(\frac{T}{10000}\right)^2\right] \exp\left(-\frac{20100}{T}\right)$		54
D_46	$\text{D}_2 + \text{H}^+ \rightarrow \text{D}_2^+ + \text{H}$	the same as for H_10		52
D_47	$\text{HD} + \text{D} \rightarrow \text{D}_2 + \text{H}$	$1.15 \times 10^{-11} \exp\left(-\frac{3220}{T}\right)$		44
D_48	$\text{D}_2 + \text{H} \rightarrow \text{HD} + \text{D}$	$\text{dex}[-86.1558 + 4.53978 \log T + 33.5707(\log T)^2 - 13.0449(\log T)^3 + 1.22017(\log T)^4 + 0.0482453(\log T)^5]$	$T \leq 2200 \text{ K}$	43
		$2.67 \times 10^{-10} \exp\left(-\frac{5945}{T}\right)$	$T > 2200 \text{ K}$	
D_49	$\text{HD} + \gamma \rightarrow \text{H} + \text{D}$	$1.19 \times 10^7 T_R^{0.28} \exp\left(-\frac{145310}{T_R}\right)$		55
D_50	$\text{D}_2^+ + \gamma \rightarrow \text{D} + \text{D}^+$	the same as for H_08		
D_51	$\text{D}_2 + \gamma \rightarrow \text{D}_2^+ + \text{e}^-$	the same as for H_14		
D_52	$\text{D}_2 + \gamma \rightarrow \text{D} + \text{D}$	the same as for H_15		
D_53	$\text{D}^- + \gamma \rightarrow \text{D} + \text{e}^-$	the same as for H_04		
D_54	$\text{HD} + \text{H}_3^+ \rightarrow \text{H}_2 + \text{H}_2\text{D}^+$	$1.0 \times 10^{-9} (2.1 - 0.4 \cdot \log(T))$		3
D_55	$\text{D}_2 + \text{e}^- \rightarrow \text{D} + \text{D} + \text{e}^-$	$8.24 \times 10^{-9} T^{0.126} \exp\left(-\frac{105388}{T}\right)$ $2.75 \times 10^{-9} T^{0.163} \exp\left(-\frac{53339.7}{T}\right)$	$v = 0$ LTE	20
D_56	$\text{HD}^+ + \text{H}_2 \rightarrow \text{H}_3^+ + \text{D}$	the same as for H_13		
D_57	$\text{H}_2\text{D}^+ + \text{H}_2 \rightarrow \text{H}_3^+ + \text{HD}$	$4.7 \times 10^{-9} \exp\left(-\frac{215}{T}\right)$	$T < 100 \text{ K}$	3
		5.5×10^{-10}	$T \geq 100 \text{ K}$	
D_58	$\text{D} + \text{e}^- \rightarrow \text{D}^+ + \text{e}^- + \text{e}^-$	the same as for H_20		52

Continued on next page

Table B.1 – continued from previous page

Tag	Reaction	Rate coefficient (cm ³ s ⁻¹ , cm ⁶ s ⁻¹ , s ⁻¹)		Ref.
D_59	HD + e ⁻ → D + H ⁻	$1.35 \times 10^{-9} T^{-1.27} \exp\left(-\frac{43000}{T}\right)$	ν = 0 LTE	56
D_60	HD + e ⁻ → H + D ⁻	$1.35 \times 10^{-9} T^{-1.27} \exp\left(-\frac{43000}{T}\right)$		56
D_61	HD + e ⁻ → H + D + e ⁻	$5.09 \times 10^{-9} T^{0.128} \exp\left(-\frac{103258}{T}\right)$		57
D_62	H ₂ + D ⁺ → H ₂ ⁺ + D	the same as for H_10	T ≤ 10000 K T > 10000 K	52
D_63	H ₂ + D ⁺ → HD ⁺ + H	$\left[1.04 \times 10^{-9} + 9.52 \times 10^{-9} \left(\frac{T}{10000}\right) - 1.81 \times 10^{-9} \left(\frac{T}{10000}\right)^2\right] \exp\left(-\frac{21000}{T}\right)$		54
D_64	HD + H ⁺ → HD ⁺ + H	the same as for H_10		52
D_65	HD + H → H + D + H	the same as for H_19		18
D_66	HD + He → H + D + He	the same as for H_30		18
D_67	HD + He ⁺ → HD ⁺ + He	the same as for He_20		52
D_68	HD + He ⁺ → He + H ⁺ + D	$1.85 \times 10^{-14} \exp\left(\frac{35}{T}\right)$		49
D_69	HD + He ⁺ → He + H + D ⁺	$1.85 \times 10^{-14} \exp\left(\frac{35}{T}\right)$		49
D_70	HD ⁺ + D → HD + D ⁺	the same as for H_09		52
D_71	D ₂ + e ⁻ → D + D ⁻	$6.7 \times 10^{-11} T^{-1.27} \exp\left(-\frac{43000}{T}\right)$		56
D_72	D ⁻ + e ⁻ → D + e ⁻ + e ⁻	the same as for H_31		52
D_73	D ⁻ + H → D + H + e ⁻	the same as for H_32		52
D_74	D ⁺ + H ⁻ → D + H	the same as for H_06		52
D_75	D ⁺ + D ⁻ → D + D	the same as for H_06		52
D_76	H ₂ ⁺ + D ⁻ → H ₂ + D	$1.7 \times 10^{-7} \left(\frac{T}{300}\right)^{-0.5}$		45
D_77	H ₂ ⁺ + D ⁻ → H + H + D	$1.7 \times 10^{-7} \left(\frac{T}{300}\right)^{-0.5}$		45
D_78	HD ⁺ + H ⁻ → HD + H	$1.5 \times 10^{-7} \left(\frac{T}{300}\right)^{-0.5}$		45
D_79	HD ⁺ + H ⁻ → D + H + H	$1.5 \times 10^{-7} \left(\frac{T}{300}\right)^{-0.5}$		45
D_80	HD ⁺ + D ⁻ → HD + D	$1.9 \times 10^{-7} \left(\frac{T}{300}\right)^{-0.5}$	45	
D_81	HD ⁺ + D ⁻ → D + H + D	$1.9 \times 10^{-7} \left(\frac{T}{300}\right)^{-0.5}$	45	
D_82	D ₂ ⁺ + H ⁻ → D ₂ + H	$1.5 \times 10^{-7} \left(\frac{T}{300}\right)^{-0.5}$	45	
D_83	D ₂ ⁺ + H ⁻ → D + D + H	$1.5 \times 10^{-7} \left(\frac{T}{300}\right)^{-0.5}$	45	
D_84	D ₂ ⁺ + D ⁻ → D ₂ + D	$2.0 \times 10^{-7} \left(\frac{T}{300}\right)^{-0.5}$	45	
D_85	D ₂ ⁺ + D ⁻ → D + D + D	$2.0 \times 10^{-7} \left(\frac{T}{300}\right)^{-0.5}$	45	
D_86	D + D ₂ ⁺ → D ₂ + D ⁺	the same as for H_09	52	
D_87	HD + D ⁺ → HD ⁺ + D	the same as for H_10	52	
D_88	HD + D ⁺ → D ₂ ⁺ + H	$\left[3.54 \times 10^{-9} + 7.50 \times 10^{-10} \left(\frac{T}{10000}\right) - 2.92 \times 10^{-10} \left(\frac{T}{10000}\right)^2\right] \exp\left(-\frac{21100}{T}\right)$	54	
D_89	D ₂ + H ⁺ → HD + D ⁺	$2.1 \times 10^{-9} \exp\left(-\frac{491}{T}\right)$	53	
D_90	D ₂ + D ⁺ → D ₂ ⁺ + D	the same as for H_10	52	
D_91	HD + H ₂ → H + D + H ₂	the same as for H_29 but with $n_{cr} \rightarrow 100n_{cr}$	18	
D_92	D ₂ + H → D + D + H	the same as for H_19	52	
D_93	D ₂ + H ₂ → D + D + H ₂	the same as for H_29	52	
D_94	He + D ⁺ → D + He ⁺	$1.85 \times 10^{-9} T^{-0.75} \exp\left(-\frac{127500}{T}\right)$	45	
D_95	He ⁺ + D → D ⁺ + He	$5.9 \times 10^{-37} T^{4.74}$	45	
D_96	D ⁻ + He → D + He + e ⁻	$1.1 \times 10^{-15} \left(\frac{T}{300}\right)^{0.25}$	45	
D_97	He ⁺ + D ⁻ → He + D	$1.5 \times 10^{-17} T^2 \exp\left(-\frac{19870}{T}\right)$	45	
D_98	D ₂ + He ⁺ → D ₂ ⁺ + He	$3.03 \times 10^{-7} \left(\frac{T}{300}\right)^{-0.52} \exp\left(\frac{T}{22400}\right)$	45	
D_99	D ₂ + He ⁺ → He + D ⁺ + D	2.5×10^{-14}	53	
D_100	D ₂ + He → D + D + He	$1.1 \times 10^{-13} T_3^{-0.24}$	53	
		the same as for H_30	52	

Note: T and T_{eV} are the gas temperature in units of K and eV respectively. References are to the primary source of data for each reaction. Reactions with a peak contribution to the synthesis or destruction of any reactant exceeding 0.1 % are bolded.

References:

1: Seager et al. (1999), 2: Wishart (1979), 3: Galli & Palla (1998), 4: Croft et al. (1999), 5: Ramaker & Peek (1976), 6: Karpas et al. (1979), 7: Savin et al. (2004), 8: Poulaert et al. (1978), 9: Coppola et al. (2011), 10: Theard & Huntress (1974), 11: Novosyadlyj et al. (2022), 12: Mac Low & Shull (1986), 13: Lepp & Shull (1983), 14: Janev et al. (1987), 15: this paper: Fit based on cross-section from <https://home.strw.leidenuniv.nl/~ewine/photo/>, 16: Méndez et al. (2006), 17: Janev et al. (2003), 18: Glover & Abel (2008), 19: Schulz & Asundi (1967), 20: Trevisan & Tennyson (2002a), 21: Martin et al. (1998), 22: Shapiro & Kang (1987), 23: Dove et al. (1987), 24: Dalgarno & Lepp (1987), 25: Walkauskas & Kaufman (1975), 26: Albertsson et al. (2014), 27: Soon (1992), 28: Database of kinetic data of interest for astrochemical (KIDA, kida.astrochem-tools.org), 29: Courtney et al. (2021), 30: De Fazio (2014), 31: Coppola et al. (2017), 32: Ferland et al. (1992), 33: Kimura et al. (1993), 34: Zygelman et al. (1989), 35: Black (1978), 36: Peart & Hayton (1994), 37: this paper: Fit to data from Schauer et al. (1989); Johnsen et al. (1980) 38: Glover & Abel (2008); Barlow S. G. , 1984, PhD thesis, Univ. Colorado 39: Huq et al. (1982), 40: Savin (2002), 41: Lindinger et al. (1982), 42: Dickinson (2005), 43: Fit of Glover & Abel (2008) to data from Mielke et al. (2003), 44: Shavitt (1959), 45: Same as corresponding H reaction, but scaled by D reduced mass (see Glover & Abel (2008)), 46: Strömholm et al. (1995), 47: Datz et al. (1995); Larsson et al. (1996), 48: Dalgarno & McDowell (1956), scaled by D reduced mass (see Glover & Abel (2008)), 49: Same as corresponding H reaction, with branching ratio assumed uniform (see Glover & Abel (2008)), 50: estimate from Glover & Abel (2008), 51: Linder et al. (1995), 52: Same as corresponding H reaction (see Glover & Abel (2008)), 53: Walmsley et al. (2004), 54: Fit of Glover & Abel (2008) based on cross-section from Wang & Stancil (2002) 55: Coppola et al. (2011), 56: Xu & Fabrikant (2001), 57: Trevisan & Tennyson (2002b), 58: Adams & Smith (1985), 59: Stancil et al. (1998).

Table B.2. Map of chemical reactions.

	e	p	H	H ⁻	H ₂	H ₂ ⁺	H ₃ ⁺	He	He ⁺	He ⁺⁺	HeH ⁺	D	D ⁻	D ⁺	D ₂	D ₂ ⁺	HD	HD ⁺	H ₂ D ⁺	γ	
e	-	H_02 H_20 H_23 H_26 H_41 H_42	H_04 H_28 H_31 H_32 H_40 H_41 H_42 He_21 D_61 D_73	-	H_05	H_11 H_14 H_40	-	He_21 D_96	He_02 He_15	He_07 He_16	-	D_53 D_54 D_61 D_72 D_73 D_96	-	D_02 D_58	D_31	D_34 D_51	D_22 D_23	D_32 D_33	-	-	
p	H_01	H_26	H_08 H_37 H_38 H_41 H_42 He_19	-	H_09 H_21 H_24	-	-	He_05 He_09 He_19 D_68	-	-	-	D_04 D_26 D_68	-	-	D_40 D_41 D_44	-	D_05 D_09 D_38	-	-	-	
H	H_03 H_20 H_23	H_07 H_24 H_43	H_06 H_12 H_15 H_19 H_22 H_25 H_28 H_32 H_34 H_35 H_36 H_37 H_38 H_42 D_17 D_65 D_77	H_27	H_17 H_25 H_29 H_33 D_91	H_10 H_40 H_43	H_13 H_39	H_30 He_12 He_17 He_19 He_21 D_66 D_69	He_08 He_14 He_22	-	-	He_10	D_14 D_17 D_35 D_49 D_61 D_65 D_66 D_73 D_74 D_77 D_79 D_81 D_83 D_91 D_92	D_30 D_60	D_03 D_13 D_69	D_47 D_82	D_39 D_46 D_88	D_08 D_19 D_78	D_27 D_63 D_64	D_15 D_16	H_01
H ⁻	H_31	H_06 H_11	H_05 H_32	-	-	-	-	-	-	-	-	D_29 D_59	-	-	-	-	-	-	-	H_03	
H ₂	H_27 H_28	H_10 H_18 H_38	H_19 H_35	-	H_29 H_35 H_44	H_16	-	H_36	-	-	-	D_10 D_18 D_76 D_91 D_93	-	D_06 D_25 D_37	-	-	-	-	-	D_55	-
H ₂ ⁺	H_12 H_41	-	H_09 H_37	H_33 H_34	H_13	-	-	He_04 He_20	-	-	-	D_21 D_24 D_62	-	-	-	-	-	-	-	-	H_07
H ₃ ⁺	H_17 H_22 H_40	-	H_16	H_44	H_39	-	-	He_13	-	-	-	D_20 D_56	-	-	-	-	D_57	-	-	-	H_18
He	He_15	He_03 He_08 He_18	H_36	He_21	H_30	He_10	-	-	-	-	-	D_66 D_68 D_96 D_97 D_99 D_100	-	D_69 D_95 D_99	-	D_98	-	D_67	-	He_01	
He ⁺	He_01 He_16	-	He_09 He_11	He_17	He_19 He_20 He_22	-	-	-	-	-	-	D_94	-	-	-	-	-	-	-	-	He_06
He ⁺⁺	He_06	-	-	-	-	-	-	-	-	-	-	-	-	-	-	-	-	-	-	-	-
HeH ⁺	He_12	-	He_04	-	He_13	-	-	-	-	-	-	-	-	-	-	-	-	-	-	-	He_03 He_11 He_18
D	D_28 D_58	D_03 D_11	D_07	D_22 D_30	D_08	D_27 D_37 D_38	D_16	-	D_95	-	-	D_52 D_54 D_75 D_81 D_83 D_85 D_92	D_71	D_50 D_99	D_84	D_90	D_48 D_80	D_42 D_45 D_87	-	-	D_01
D ⁻	D_72	D_32 D_35	D_23 D_29 D_73	-	-	D_76 D_77	-	D_96	D_97	-	-	D_31	-	-	-	-	-	-	-	-	D_28
D ⁺	D_01	-	D_04 D_12	D_33 D_74	D_05 D_62 D_63	-	-	D_94	-	-	-	D_36	D_34 D_75	-	D_86	-	D_43 D_70 D_89	-	-	-	-
D ₂	D_54 D_71	D_45 D_46 D_89	D_48 D_92	-	D_93	-	-	D_100	D_98 D_99	-	-	-	-	-	D_90	-	-	-	-	-	-
D ₂ ⁺	-	-	D_41 D_42 D_43	D_82 D_83	-	-	-	-	-	-	-	D_86	D_84 D_85	-	-	-	-	-	-	-	D_36
HD	D_59 D_60 D_61	D_06 D_24 D_64	D_10 D_65	-	D_91	-	D_55	D_66	D_67 D_68 D_69	-	-	D_47	-	D_44 D_87 D_88	-	-	-	-	-	-	D_07
HD ⁺	D_14	-	D_09 D_21 D_25	D_78 D_79	D_15 D_56	-	-	-	-	-	-	D_39 D_40 D_70	D_80 D_81	-	-	-	-	-	-	-	D_11 D_12
H ₂ D ⁺	D_17 D_18 D_19	-	D_20	-	D_57	-	-	-	-	-	-	-	-	-	-	-	-	-	-	-	-
γ	-	He_18	H_02	H_04	H_14 H_15	H_08 H_26	H_21	He_02 He_18	He_07	-	He_05 He_14	D_02	D_53	-	D_51 D_52	D_50	D_49	D_13 D_26	-	-	-

Note: Red and orange labels indicate reactions where reactants are destroyed, while blue and cyan show reactions where reactants are synthesized. Red and blue correspond to reactions with four reactants, and other colours to those with more.